Applied Geochemistry 162 (2024) 105907

Contents lists available at ScienceDirect

Applied Geochemistry

journal homepage: www.elsevier.com/locate/apgeochem

Temperature-dependent adsorption by goethite of molybdate and vanadate

Michael Kersten

Geosciences Institute, Johannes Gutenberg-University, 55099, Mainz, Germany

ARTICLE INFO

Editorial handling by: Jon Petter Gustafsson

Keywords:
Surface complexation
CD-MUSIC
Exothermic
Endothermic
Inner-sphere
Outer-sphere

ABSTRACT

Goethite, a common Fe(III) oxyhydroxide found in soils and aquifers, is employed in water purification technology due to its high oxo-anion adsorption capacity. In a series of batch equilibrium experiments, goethite suspensions were subjected to varying ionic strengths, concentrations of vanadate and molybdate, and pH values ranging from 3 to 10. These experiments were also carried out at four distinct temperatures, ranging from 10 to 75 °C. The results from over 1400 individual batch equilibrium experiments revealed that the adsorption of vanadate and molybdate generally decreases as the pH increases, as is typically observed for anion adsorption envelopes. However, this decrease was found to be less pronounced for vanadate compared to molybdate, with only the latter showing a sharp adsorption envelope decline at circumneutral pH values near the point of zero charge of the goethite surface. To interpret these findings, the Charge Distribution Multisite Surface Complexation (CD-MUSIC) model framework was employed. According to the model fit, the adsorption of molybdate is primarily governed by an outer-sphere surface complex at circumneutral pH conditions, which remains relatively unaffected by temperature variations, indicating a nearly zero enthalpy of reaction. Similarly, for vanadate, there was also no significant temperature effect, but the reasons differed. For the two inner-sphere vanadate surface complexes, a linear decrease in log*K* values with temperature was observed, suggesting an exothermic adsorption reaction with negative enthalpy as typical for inner-sphere binding of oxyanions. This was counterbalanced by an increase in log*K* with temperature for the strong dioxovanadium(V) cation surface complex, which exhibited a positive enthalpy and thus an endothermic reaction typical for cations. As a result, the overall uptake of vanadate by goethite was found to be almost temperature independent as well.

1. Introduction

Environmental issues with molybdenum (Mo) and vanadium (V) have not often been reported, although they are common metal contaminants released into wastewater from industrial plants and other anthropogenic sources, including coal combustion residues (Harkness et al., 2017). Both metals are widely used in high-performance alloyed steel production and are also important metal components for the green transition. Future developments in vanadium usage, such as the growing adoption of V-based sodium-ion batteries for energy storage, could have a significant impact on the demand for this metal (Samarin et al., 2023). However, even though they are designated as critical materials, there is currently no effective circular economy for these metals. At their end-of-life, they are treated as impurities to eliminate rather than precious metals to recover (Graedel and Miatto, 2023). Environmental contamination by these metals is therefore an ongoing issue and in particular V biogeochemistry and bioremediation have gathered increasing attention in the past decade (Zhang et al., 2023).

Molybdate and vanadate species are the most soluble forms of Mo (VI) and V(V) and can occur also as geogenic contaminations of groundwater (Smedley and Kinniburgh, 2017; Gustafsson, 2019; Parnell, 2022). Because of their high toxicity, even at low concentrations (in the μg L^{-1} range), V species in groundwater with elevated geogenic or anthropogenic concentrations can pose a significant health risk (White and Levy, 2021; Vasseghian et al., 2021). A health-based guide value in drinking water of 4 μg L^{-1} has been set by the German Environment Agency. Health problems due to elevated geogenic V and Mo concentrations in groundwater may be exacerbated by co-occurrence with other toxic oxo-anions, as has been found in the eastern United States (Coyte and Vengosh, 2020). Elevated V groundwater concentrations up to 0.2 mg L^{-1} have been detected in volcanic areas worldwide (Hamada, 1998; Arena et al., 2015; Koh et al., 2016). In Argentina, elevated geogenic V concentrations have also been observed to correlate with increased levels of silicic acid and arsenic in Tertiary and Quaternary fluvial and aeolian (alluvial) deposits. The potential sources were identified as volcanic ash layers containing up to 90% rhyolitic glass

E-mail address: kersten@uni-mainz.de.

https://doi.org/10.1016/j.apgeochem.2024.105907
Received 1 September 2023; Received in revised form 28 December 2023; Accepted 13 January 2024
Available online 17 January 2024

dispersed in the sediments (Bundschuh et al., 2004; Bhattacharya et al., 2006). Similarly, in the semi-arid Province of La Pampa, Argentina, 40% of analyzed groundwater samples have concentrations above the World Health Organization (WHO) health-based value of 70 μg L^{-1} (Smedley and Nicolli, 2014), with a maximum value of 1715 μg L^{-1} ever measured in groundwater unaffected by anthropogenic activities (Nicolli et al., 1989). Dissolution of mafic phenocrysts common in the local tuffaceous aquifer rocks has been identified as a likely source of groundwater V in Oasis Valley (Nevada, USA; Telfeyan et al., 2015). Fluorapatite with up to 10% phosphate substitution by vanadate was identified as the primary geogenic source in a German volcanic area (Härter et al., 2020). Many other groundwater data are provided by a recent compilation (Zhang et al., 2023).

Once released into the aqueous environment, molybdate and vanadate in aquifers tend to be sorbed to Fe/Mn oxyhydroxides (Gustafsson, 2019; Yang and Wang, 2021; Zhang et al., 2023). As a mitigation option for groundwater V and Mo contamination, in-situ co-precipitation by oxidation of Fe(II)-bearing anoxic groundwater or adsorption onto fixed bed adsorbers based on Fe oxyhydroxides are often applied (Weidner and Ciesielczyk, 2019; Dabizha et al., 2020; Leiviskä, 2021; Mahringer et al., 2023). Column and field tests related to aquifer thermal energy storage (ATES) found significantly elevated Mo, V, and other oxo-anions after hot water injection into the shallow aquifer that could not be explained simply by reductive dissolution of Fe oxyhydroxide adsorbent phases (Bonte et al., 2013, 2014; Lüders et al., 2021; Craig et al., 2021). Based on batch tests, it was hypothesized that the significant temperature-induced change in oxo-anion mobility could be related to a thermal desorption process (Lüders et al., 2021). However, for an accurate prediction of the concentration changes, there is a lack of thermodynamic parameters to prove the hypothesis of a temperature dependent adsorption-desorption mechanism.

Surface complexation models can be used to interpret experimental data, describe the adsorption processes, and estimate ion partitioning at the solid/solution interface. Despite the increasing number of published modeling studies on oxo-anion surface complexation, such as molybdate and vanadate (e.g., Gustafsson, 2003; Xu et al., 2006; Gustafsson and Tiberg, 2015; Larsson et al., 2017; Brinza et al., 2019; Wang and Sherman, 2021; Dabizha et al., 2020), the impact of temperature on adsorption has received limited attention. Quantitative standard molar enthalpy and entropy data for the molybdate and vanadate surface complexation reactions with (hydr)oxides are not yet available, but a comprehensive set of temperature-dependent surface complexation constants would be highly valuable for various applications, including (i) the removal of Mo and V from hot industrial wastewaters, (ii) the study of Mo/V-containing canister materials in underground nuclear waste repositories with long-term residual heat generation by fuel cells, (iii) the investigation of Mo/V behavior in geothermal water plants dealing with highly saline brines and addressing corrosion issues, and (iv) the examination of Mo/V behavior during ATES activities. Therefore, the aim of this study was to provide temperature-dependent surface complexation constants for adsorption of both molybdate and vanadate by goethite (α-FeOOH). Goethite was chosen for the experiments because it is relatively inert towards temperature, at least below 100 °C, while other Fe hydroxides such as ferrihydrite tend to change their structure and amount of specific surface due to temperature-induced ageing.

2. Materials and methods

2.1. Batch adsorption experiments

All chemicals used were of analytical grade and were purchased from Merck (Darmstadt, Germany). All aqueous phase solutions and suspensions were prepared using purified water (Milli-Q, Merck, Darmstadt, Germany) with a resistivity of 18.2 MΩ·cm at 25 °C. Argon gas was bubbled through the water to avoid contamination with CO_2, as carbonate is known to interfere with oxo-anion adsorption (Villalobos et al., 2009). Synthetic goethite was prepared from ferric nitrate solution under alkaline conditions. Briefly, 40 g $Fe(NO_3)_3{\cdot}9H_2O$ was diluted in 100 mL of water, and 28 g NaOH was dissolved in 1300 mL of water and heated to 70 °C. The iron nitrate solution was slowly added to the stirred hot NaOH solution and then aged at 90 °C for another seven days. The aged goethite phase had a relatively low Brunauer–Emmett–Teller (BET) specific surface area of 25 ± 3 m^2 g^{-1} as measured by N_2 adsorption (Quantachrome NOVA 1200, Anton Paar GmbH, Germany). A typical needle-like submicrometer crystallinity with a low amount of capping face areas was found by TEM-based imaging (Fig. S1, Supporting Information). No phase transition of this goethite to hematite was found even after heating the suspension to 140 °C overnight in a closed autoclave, as analyzed by X-ray diffraction (Fig. S2), and no Fe dissolution was found at pH values > 3 (total dissolved Fe < 10 nmol L^{-1}).

Batch equilibrium experiments were conducted under both acidic and alkaline pH conditions using 50 mL polypropylene centrifuge tubes containing 25 mL of a well-stirred suspension. Diluted goethite suspensions (5.00 g L^{-1}) were prepared in 10, 50, and 100 mM $NaNO_3$ solutions as the background electrolyte at a pH 3. The suspensions had a low enough density, as determined by Oman et al. (2007), to prevent any suspension effect on pH measurements. Stock solutions of $Na_2MoO_4{\cdot}H_2O$ or Na_3VO_4 (Merck) were added to the suspensions to give a total concentration of 10, 50, and 100 μmol L^{-1} for molybdate, or 0.1, 0.3, and 0.5 mmol L^{-1} for vanadate at a pH 3. The pH was adjusted by adding drops of 0.1 M NaOH prepared from Titrisol stock standard solution (Merck, Darmstadt, Germany) using CO_2-free boiled deionized water. The pH of a given suspension was determined using an Inolab Level 2P pH meter (WTW, Weilheim, Germany) equipped with a SenTix81 combination electrode and a temperature probe. The electrode was calibrated using CertiPur pH 4.01, 7.00, and 9.00 buffer solutions (Merck) at their respective temperatures, considering the known temperature dependence of the pH of these buffers (Covington et al., 1985). The pH was considered stable if the measured drift was ≤1 mV per minute during a 10-min period to avoid silicic acid and CO_2 contamination. The electrode was rinsed with reagent-grade HCl between samples to avoid sample cross-contamination. Together with the linearity criterion, an overall uncertainty of <0.1 pH unit was achieved in the pH measurements, as recommended by IUPAC for measurements over a wide range of unknown pH values (Naumann et al., 2002).

All centrifuge tubes were capped and placed in a thermostatically controlled water bath at the specified temperature (10, 25, 50, or 75 °C). After 72 h, the final pH of the supernatants was determined and used as input for the model fitting process. The tubes were then centrifuged at 1100 g for 20 min, whereby they cooled down. However, significant concentration changes were not expected due to quick separation of both phases. Subsequently, the supernatants were additionally passed through a 0.2 μm membrane filter syringe. The total dissolved Mo and V concentrations in the supernatants were determined using an Agilent 7700 inductively coupled plasma mass spectrometer (ICP-MS, Agilent Technologies, Santa Clara, CA, USA) with a detection limit of about 0.01 μg L^{-1}. For the measurements, each solution after filtration was diluted 100-fold with acidified water to mitigate interference by the background electrolyte. The concentrations of the blank samples were checked using the acidified water to verify accuracy. The amount of Mo and V that had been adsorbed was defined as the difference between the total initial Mo concentration and the concentration in the supernatant filtrate after equilibration and is presented here as the percentage of molybdate and vanadate adsorbed. Experimental data were thus obtained from more than 1400 individual batch experiments.

2.2. Surface complexation model

A unique feature of the 1-p*K* three-plane CD-MUSIC surface complexation model developed by Hiemstra and Van Riemsdijk (1996) is that surface complexes can be positioned between the different surface

electrostatic planes, most commonly between the two innermost (0- and β-) planes. Charges of surface complexes can be positioned in either of these planes or distributed between them to distinguish between inner- and outer-sphere complexation characteristics. This is achieved in the model by providing the Boltzmann factors for the two planes, and commonly not done by fitting but by accounting for the charge distribution (CD values) of the surface complexes according to Pauli's rules. A multisite surface complexation (MUSIC) with singly and triply coordinated O(H) groups, denoted ≡ $FeOH^{-1/2}$ and ≡ $Fe_3O^{-1/2}$, is used to describe the surface protonation reaction. The site densities fixed at 3.4 and 2.7 nm^{-2}, respectively, are commonly used as a standard in CD-MUSIC modeling of goethite. Clearly, there are an infinite number of combinations of specific surface area (SSA), crystal plane contribution, surface site and charge densities, capacitance values, and equilibrium constants that can fit a given set of experimental data equally well (Han and Katz, 2019). Total ion-reactive site densities ranging from 3.1 to 9.7 nm^{-2} have been reported for different goethite preparations resulting in different crystal morphologies (Villalobos et al., 2009). Sverjensky (2003) has suggested using $100{\cdot}10^{18}$ sites g^{-1} as a standard for all mineral surfaces, but we prefer to use the CD-MUSIC goethite standard as proposed by Hiemstra and Van Riemsdijk (1996).

The pH dependence of oxo-anion adsorption is mainly controlled by interactions with protons. To quantify the surface protonation reaction, the logK_H value at room temperature (25 °C) was set equal to the bulk point of zero charge, pH_{pzc} = 9.1, as determined by previous batch titrations and electroacoustic measurements for goethite samples prepared by the same procedure (Kersten and Vlasova, 2009). The 1-pK model provides a sufficiently accurate description of the titration behavior of the goethite solid-water interface (Borkovec, 1997). However, the pH_{pzc} of individual goethite crystal planes may differ from the bulk pH_{pzc} used in this study (Hiemstra and Van Riemsdijk, 1996; Gaboriaud and Ehrhardt, 2003; Boily, 2012; Han and Katz, 2019; Zhang et al., 2021), and it has been shown that various published assumptions with respect to the goethite morphology do not significantly affect the final 1-pK model bulk parameters (Lützenkirchen et al., 2008).

The background electrolyte $NaNO_3$ was accounted for by symmetric outer-sphere surface complexation of the monovalent electrolyte cation and anion, assuming that adsorption occurs in the outer Stern layer with equilibrium reaction constants fixed at $\log K_{Na} = \log K_{NO3} - \log K_H = -0.6$ for all surface sites (Hiemstra and Van Riemsdijk, 1996; Lützenkirchen et al., 2008). The binding of electrolyte ions to the surface was thus assumed to be the same for the cation and anion. This adsorption symmetry assumption is reasonable since the ionic strength was low in all experiments, and a small asymmetry has been suggested between Na^+ and NO_3^- adsorption (Hiemstra and Van Riemsdijk, 2006). Consequently, protonation and deprotonation of surface sites is assumed to be the predominant process leading to surface charge at the hydroxide surface in pure electrolyte solution (i.e., when no oxo-anions are adsorbed). Under this constraint, it is possible to use the temperature dependence of the point-of-zero-salt effect (pH_{pzse}) as a method for determining the enthalpy of the protonation process (Kersten and Vlasova, 2009). The inner-Helmholtz capacitance value depends on the type of electrolyte used. A value of C_1 = 1.0 F m^{-2} was found based on acid-base titration data in $NaNO_3$ electrolyte solutions (Kersten and Vlasova, 2009) and is within 10% of many other reported goethite studies reported (Han and Katz, 2019). The capacitance of the outer-Helmholtz layer (C_2) was set equal to C_1.

Changes in the permittivity of the water with temperature are implemented in the Visual MINTEQ code, which contains a temperature correction function for the relative permittivity such that it is 84 at 10 °C, 78 at 25 °C, 70 at 50 °C, and 62 at 75 °C (Gustafsson, pers. commun.). Temperature dependence of the inner capacitance parameter C_1 has been neglected. Kulik (2000) found a significant increase in the density of adsorbed $NaNO_3$ electrolyte ions already at moderate temperatures (50–80 °C) and ionic strength (0.1 M). To compensate for this effect with rutile (TiO_2), he suggested that C_1 should be increased by 0.15 F m^{-2} from 25 °C to 75 °C and modeled this effect using an equation of $C_1(T) = C_1(T_0) + 0.003(T-T_0)$, where temperature T is in degrees Celsius (T_0 = 25 °C). However, this change in the C_1 would only change the pH_{pzc} by < 0.1 units in this temperature range. In addition, Halter and Pfeifer (2001) found an even smaller decrease of 0.02 F m^{-2} for the alumina surface in the same temperature range (50–80 °C) for NaCl electrolyte solutions, which was within the error margin (i.e., insignificant). Therefore, the inner capacitance density parameter C_1 and thus also the electrostatic term were assumed to be independent of temperature to simplify the fitting exercise as also suggested earlier by Lützenkirchen and Fink (2019). Overall, it is important to emphasize that the log$K$ values determined at other temperatures than 25 °C may not be "real" constants in a strict thermodynamic sense, rather they represent conditional log$K$ values resulting from using the code with all simplifications mentioned above. However, it was not the aim to derive at such real log$K$'s but rather to compare and derive at a trend in temperature dependence, i.e., whether there is an exothermic or endothermic reaction behavior, or no change in uptake affinity at all. Therefore, calculation of thermodynamic constants such as enthalpy and entropy values from these log$K$'s using the two-term Van't Hoff equation was avoided here.

In the model fit, the change in pH_{pzc} with temperature had to be adopted manually with the data determined previously by Kersten and Vlasova (2009) and compiled in Table 2. The CD values were fixed at all temperatures to those determined at 25 °C, effectively reducing the number of fitting parameters to the two to three reaction constants (log$K$ values) at T > 25 °C. Since the CD values are the dominant parameter accounting for the slope of the adsorption envelope, which in turn is determined nearly exclusively by the CD values of the outer-sphere complex, fixing these parameters for all temperatures means also that the slope does not change with increasing temperature. The experimental data were ultimately fitted to determine the log$K$ values for molybdate and vanadate surface complexation using the Visual MINTEQ ver. 4.0 code coupled with the shell optimizer PEST code (Gustafsson, 2022). PEST minimizes the weighted sum of squared differences between model-generated log$K$ values and those estimated. This sum of weighted, squared, model-to-measurement discrepancies is referred to as the "objective function" (Doherty, 2015). In the PEST optimization process, the contribution of different subgroups to this objective function is calculated. A set of initial log$K$ values near to those expected (or suggested in previous publication) for the surface complexes must be supplied to PEST before each run. During the optimization, PEST modifies the log$K$ values (2–3 for the CD-MUSIC fit) that are to be optimized, passes them back to the Visual MINTEQ code, which provides a new set of model-generated values, PEST modifies the log$K$ values again, etc., until the objective function is minimized. Apart from the value of the objective function, PEST also reports the correlation coefficient R as an goodness-of-fit parameter, which is independent of the number of observations in the parameter estimation process, and it is also independent of the absolute levels of uncertainty of the observations (unlike the objective function). The uncertainty parameter R is defined as (Gustafsson, 2022):

$$R = \frac{\sum(w_i c_i - m)(w_i c_{0i} - m_0)}{[\sum(w_i c_i - m)(w_i c_i - m)\sum(w_i c_{0i} - m_0)(w_i c_{0i} - m_0)]^{1/2}} \quad (1)$$

where c_i is the i-th observation value, c_{0i} is the model-generated counterpart to the i-th observation value, m is the mean value of the weighted observations, m_0 is the mean of model-generated counterparts to observations, and w_i is the weight associated with the i-th observation. As recommended, R should be > 0.9 for an acceptable model fit (Bachmaf and Merkel, 2011; Doherty, 2015). For a more accurate temperature correction of the water dissociation reaction, an analytical expression is implemented in the Visual MINTEQ code as follows:

$$\log K_H(T) = A + B{\cdot}T + C/T + D\log T + E/T^2 \quad (2)$$

with parameters as compiled in Table 1. Such a temperature correction was also taken from the THERMODDEM database (https://thermoddem.brgm.fr/) for aqueous Mo(VI) and V(V) complexes where available (Table 1), otherwise a one-term van't Hoff extrapolation with $\Delta_r H^0$ values ($\Delta_r C^0_{p,T} = \Delta_r S^0_T = 0$) taken from Cruywagen (2000) was kept as default in the Visual MINTEQ database.

The geochemistry of V is quite complex, with three oxidation states (III, IV, and V) that can occur under natural conditions in aquifers (Shaheen et al., 2019). The thermodynamic database has been updated by the Visual MINTEQ code developer based on an extensive review of the V biogeochemistry (Gustafsson, 2019). Thermodynamic modeling predicts that dissolved MoO_4^{-2} and $H_2VO_4^-$ species dominate between pH 4–9, when dissolved concentrations are below 0.3 mmol L^{-1} (Fig. S3). Both Mo(VI) and V(V) can also form polyoxometalate species under acidic conditions at total dissolved concentrations >1 mmol L^{-1} (Torres et al., 2014; Gustafsson, 2019; Jelinek et al., 2021), for which the database now includes all relevant species formation reaction constants. Adsorption of polyvanadate species has therefore been reported at much higher total concentrations then those used in this study (Vessey et al., 2020).

3. Results and discussion

3.1. Molybdate adsorption

A typical molybdate adsorption envelope for goethite at room temperature is plotted against pH in Fig. 1a–and a full data presentation for all concentrations, ionic strengths, and temperatures (about 700 data points) is plotted in Fig. S4. As is typical for anions, the highest amount of the oxo-anion was adsorbed to goethite at the most acidic pH values. Nearly 100% of the oxo-anion was adsorbed at pH 3 and decreased to almost 0% at the highest pH 10 studied. The adsorption envelope became steeper with a decrease from nearly 100% to zero within two pH units as the total oxo-anion concentration decreased (Fig. S4). Increasing the Mo concentration from 10 μM to 100 μM shifts the pH_{50} value from 9 to 7, i.e., towards more acidic pH values, thereby decreasing the amount of molybdate adsorbed at near-neutral pH values (Fig. S4). However, no significant adsorption envelope shift was induced by the temperature.

Two different surface complexation models have been published for the possible adsorption configurations of tetrahedral molybdate oxo-anion molecules on goethite surfaces. These are monodentate outer-sphere and bidentate inner-sphere (Gustafsson and Tiberg, 2015) or both inner-sphere monodentate and bidentate (Wang and Sherman, 2021). Both models are based on spectroscopic (EXAFS) speciation and/or ab-initio molecular dynamics (MD) simulations and were both also able to fit batch-equilibrium adsorption data. While Gustafsson and Tiberg (2015) applied an outer-sphere surface complex, as often used for oxo-anions, Wang and Sherman (2021) argued that the mono-dentate configuration should be an inner-sphere rather than an outer-sphere surface complex. However, it appears that Wang and Sherman (2021) have performed MD simulations using only a neutral (110) slab. Clearly, MD simulations using charged (protonated) slabs are challenging due to polarization effects if the electrostatic charge is not balanced (Georgieva et al., 2020). This approach limits MD simulations to the neutral surface near the point-of-zero-charge (pH_{pzc}). Quite unusual, Wang and Sherman (2021) assigned the same EXAFS peak at 3.40 Å with a poor fit and thus an extremely high *R*-factor to both the monodentate and bidentate corner-sharing surface complexes. In fact, they cannot exclude that this peak represents only the bidentate edge-sharing complex, but this was not simulated by their MD approach. In fact, the contribution of such a bidentate inner-sphere complex is negligible near the pH_{pzc} (Fig. 1a). In addition, when fitting their batch equilibrium adsorption data, they used a charge distribution for their mono-dentate reaction that is typical for a monodentate protonated inner-sphere molybdate surface complex, where a proton is added to the inner Stern layer ($\Delta z_0 = 1$) and the charge of the oxo-anion is completely located on the second Stern layer, $\Delta z_1 = -2$. However, this must be a monodentate binuclear surface complex with a second binding to the proton of a surface hydroxyl group on another surface site as proposed by Davantès et al. (2016) for molybdate adsorption onto lepidocrocite (γ-FeOOH). In fact, from the charge distribution model point of view, there is almost no difference to the model parameters of Gustafsson and Tiberg (2015), who used $\Delta z_0 = 0.8$ and $\Delta z_1 = -1.8$ for their CD-MUSIC model parameterization assuming an outer-sphere surface complex. The only difference is the loss of one water molecule in their chemical reaction, but this does not count for the law of mass action log*K* value. Therefore, it is not surprising that the log*K* values differ by no more than two units between the two models, and that the surface species distribution is quite similar. To sum up, we consider the arguments of Wang and Sherman (2021) not strong enough to exclude outer-sphere molybdate surface complexation. As discussed below, we deem just opposite the outer-sphere complexation most important for molybdate adsorption and tend therefore to follow the CD-MUSIC model of Gustafsson and Tiberg (2015) formulated by the stoichiometry below:

$$2{\equiv}FeOH^{-0.5} + MoO_4^{-2} + 2H^+ \leftrightarrow ({\equiv}FeO)_2MoO_2^- + 2H_2O \quad (3)$$

$${\equiv}FeOH^{-0.5} + MoO_4^{-2} + H^+ \leftrightarrow {\equiv}FeOH_2MoO_4^{-1.5} \quad (4)$$

In Eq. (3), the reaction consumes two H^+ to release two water molecules

Table 2
Surface complexation reaction constants (at 10 – 75 °C and 1 bar) for molybdate and vanadate adsorption by goethite as fitted to experimental data using the 1-p*K* CD-MUSIC model. The proton adsorption data were taken from Kersten and Vlasova (2009).

Surface complexation reaction	$logK_{283}$	$logK_{298}$	$logK_{323}$	$logK_{348}$
$H_2O \leftrightarrow H^+ + OH^-$	−14.54	−14.00	−13.29	−12.72
$\equiv FeOH^{-0.5} + H^+ \leftrightarrow \equiv FeOH_2^{+0.5}$	9.45	9.10	8.60	8.20
$\equiv Fe_3O^{-0.5} + H^+ \leftrightarrow \equiv Fe_3OH^{+0.5}$	9.45	9.10	8.60	8.20
$\equiv FeOH^{-0.5} + Na^+ \leftrightarrow \equiv FeOHNa^{+0.5}$	−0.6	−0.6	−0.6	−0.6
$\equiv Fe_3O^{-0.5} + Na^+ \leftrightarrow \equiv Fe_3ONa^{+0.5}$	−0.6	−0.6	−0.6	−0.6
$\equiv FeOH^{-0.5} + H^+ + NO_3^- \leftrightarrow \equiv FeOH_2NO_3^{-0.5}$	8.85	8.50	8.00	7.60
$\equiv Fe_3O^{-0.5} + H^+ + NO_3^- \leftrightarrow \equiv Fe_3OHNO_3^{-0.5}$	8.85	8.50	8.00	7.60
$\equiv FeOH^{-0.5} + MoO_4^{-2} + H^+ \leftrightarrow \equiv FeOH_2MoO_4^{-1.5}$	12.05	12.37	12.13	12.21
$2{\equiv}FeOH^{-0.5} + MoO_4^{-2} + 2H^+ \leftrightarrow (\equiv FeO)_2MoO_2^- + 2H_2O$	17.46	17.06	16.32	15.58
$2{\equiv}FeOH^{-0.5} + HVO_4^{-2} + H^+ \leftrightarrow (\equiv FeO)_2VO_2^{-2} + 2H_2O$	14.95	14.78	14.40	13.95
$2{\equiv}FeOH^{-0.5} + HVO_4^{-2} + 2H^+ \leftrightarrow (\equiv FeO)_2VOOH^- + 2H_2O$	22.25	21.97	21.40	20.80
$2{\equiv}FeOH^{-0.5} + HVO_4^{-2} + 3H^+ \leftrightarrow (\equiv FeO)_2V(OH)_2^0 + 2H_2O$	27.40	27.60	28.00	28.40

Table 1
Temperature corrections used for aqueous oxo-anion species formations according to the polynomial expression $logK(T) = A + B{\cdot}T + C/T + D\log T + E/T^2$, with temperature in Kelvin and parameters taken from the THERMODDEM (https://thermoddem.brgm.fr/) database.

Aqueous complexation reaction	$logK(T_0)$	A	B	C	D	E
$H_2O = H^+ + OH^-$	−14.00	−701.954	−0.112739	36168.09	253.600	−2423262
$MoO_4^{-2} + H^+ = HMoO_4^-$	4.40	797.837	0.128593	−45529.95	−287.642	2905031
$HVO_4^{-2} + H^+ = H_2VO_4^-$	8.05	461.769	0.076743	−19387.97	−169.705	742814
$HVO_4^{-2} + 3H^+ = VO_2^+ + 2H_2O$	15.14	627.653	0.111260	0	0	936959

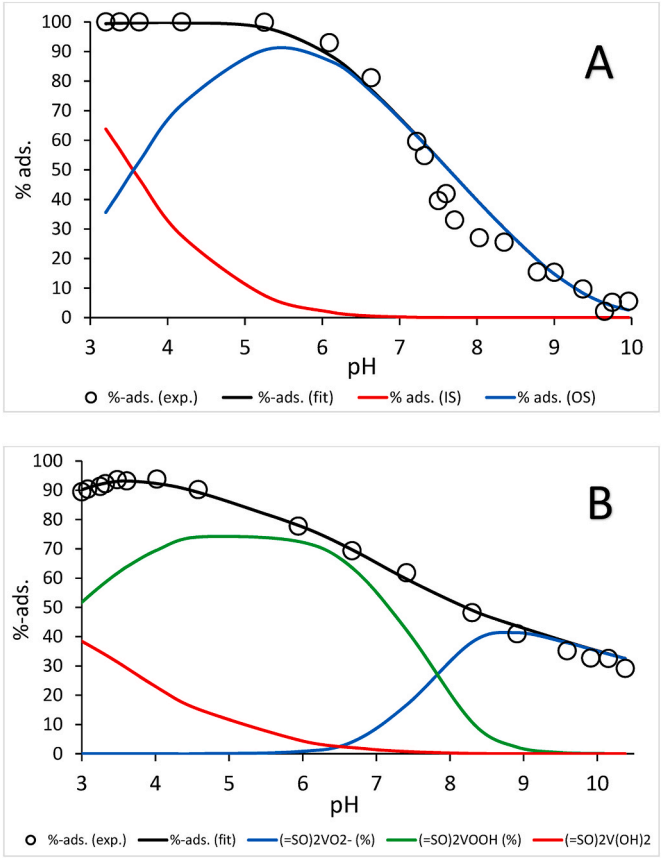

Fig. 1. (A) Percentage of adsorbed molybdate (A) and vanadate (B) plotted against pH. The total element concentration was 100 μmol L^{-1}, goethite adsorbent concentration was 5 g L^{-1}, the ionic strength was 50 mM $NaNO_3$, and the temperature was 25 °C for both cases. The curves were fitted using the CD-MUSIC adsorption model. The coloured lines represent the respective surface complexes as denoted in the legends, while the black lines represent the total adsorbed amounts.

to describe the bidentate inner-sphere surface complexation, and Eq. (4) consumes one H^+ to describe the outer-sphere surface complexation. Alternatively, one may think of the bidentate inner-sphere molybdate complexation (reaction (3)) to occur via ligand exchange with two OH^- surface functional groups and (after protonation) simultaneous release in the form of two H_2O molecules. For both surface complexation reactions, the charge distribution parameters published by Gustafsson and Tiberg (2015) were adopted, which are $\Delta z_0 = 0.5$ and $\Delta z_1 = -0.5$ for reaction (3) and $\Delta z_0 = 0.8$ and $\Delta z_1 = -1.8$ for the outer-sphere (H-bonded) complexation reaction (4). The fit results for all temperatures are compiled in Table 2.

The overall adsorption reaction is dominated by the outer-sphere surface complex of reaction (4). The logK_T values of the outer-sphere complex are almost temperature-independent, while those of the inner-sphere complex are decreasing with temperature indicating an exothermic reaction (Table 2 and Fig. 2). This is not surprising since the heat effects of outer-sphere complexes such as electrolyte ions are small to negligible and, therefore, the enthalpies of binding equal nearly zero (i.e., zero slope in the log$K_{T,OS}$ vs. T curve, Fig. 2). This is because outer-sphere complexes interact with the hydroxide surface in a predominantly electrostatic way, while any inner-sphere reaction of oxo-anions induces significant change in charging of the surface (negative $\Delta_r H$). Therefore, the latter is exothermic and becomes weaker with increasing temperature (Kulik, 2006). The significant temperature effect found on the inner-sphere model complex (red lines in Fig. 1a and S4) can be shown also by the pH at which the contributions of the inner- and

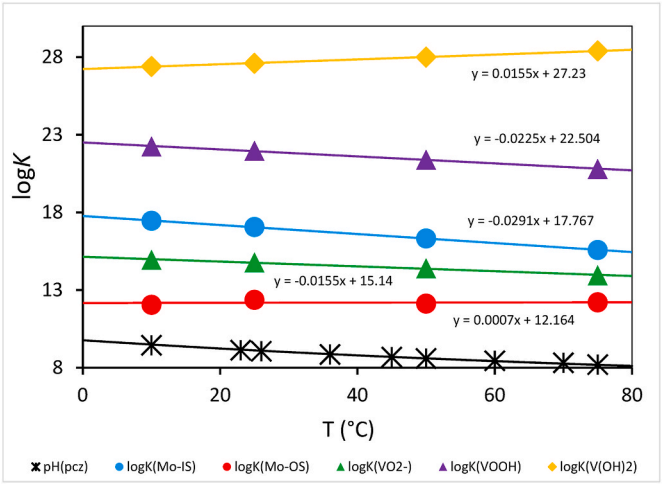

Fig. 2. Plots of the logK_T data for molybdate and vanadate surface complexation reactions (3)–(7). The asterisks represent the pH_{pzc} data published by Kersten and Vlasova (2009). The linear regressions through the data are displayed, and the regression equations are provided next to the respective lines for reference.

outer-sphere surface species became equal (i.e., the point at which the curves crossed). This point shifts to higher pH values with increasing ionic strength as to be expected due to the known negative impact of the ionic strength on the outer-sphere complexation. On the other hand, this point shifts to lower pH values with increasing temperature (Fig. 3 and S4). The latter effect indicates that temperature-dependent electrostatic properties of the goethite surface are affecting also the inner-sphere Mo adsorption. The surface acidity (pH_{pzc}) decreased with increasing temperature (Table 2), meaning that there was less shielding of the negative charges of the surface complexes (i.e., more repulsion) as the temperature increased. This shifted the inner-sphere oxo-anion adsorption toward the acidic region by approximately 0.25 pH units per 10 °C, as previously found for selenate (Kersten and Vlasova, 2013) and chromate (Dabizha and Kersten, 2020). Finally, the inner-sphere complex nearly vanishes at 75 °C in the pH > 3 region studied here (see Fig. S4d).

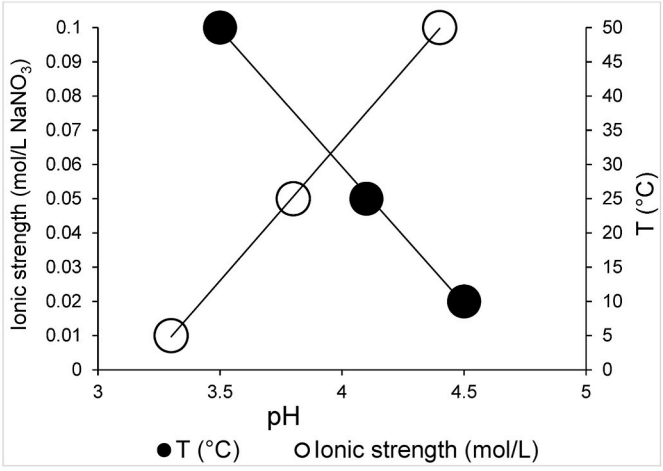

Fig. 3. Location of the crossing point of equal amount of outer- and inner-sphere molybdate surface complex formation on the pH scale in dependence of the ionic strength (for 10 μmol L^{-1} molybdate at 10 °C, open dots) and of the temperature (for 0.1 mmol L^{-1} molybdate at $I = 0.1$ M, black dots). The size of the dots represents the data error margins.

3.2. Vanadate adsorption

An exemplary vanadate adsorption envelope is plotted against pH for room temperature, the lowest total concentration of 100 μmol L^{-1}, and a fixed ionic strength in Fig. 1b. Data for all other concentrations, ionic strengths, and temperatures are presented in Fig. S5. Unlike for molybdate, no impact of the ionic strength was found on the vanadate adsorption envelope. Accordingly, no outer-sphere but solely inner-sphere surface complexation has been proposed for vanadate, for example, in bidentate corner-sharing (Peacock and Sherman, 2004), or more recently in bidentate edge-sharing coordination (Larsson et al., 2017; Abernathy et al., 2022). Neither of these researchers found any evidence for monodentate inner-sphere surface complex formation using EXAFS measurements. The CD-MUSIC model by Larsson et al. (2017), which utilizes this bidentate complex with different degrees of protonation to account for various vanadate species (see Fig. S3), was adopted by the stoichiometry shown below:

$$2{\equiv}FeOH^{-0.5} + HVO_4^{-2} + H^+ \leftrightarrow ({\equiv}FeO)_2VO_2^{-2} + 2H_2O \quad (5)$$

$$2{\equiv}FeOH^{-0.5} + HVO_4^{-2} + 2H^+ \leftrightarrow ({\equiv}FeO)_2VOOH^- + 2H_2O \quad (6)$$

$$2{\equiv}FeOH^{-0.5} + HVO_4^{-2} + 3H^+ \leftrightarrow ({\equiv}FeO)_2V(OH)_2^0 + 2H_2O \quad (7)$$

The CD values of $\Delta z_0 = 1.0$ and $\Delta z_1 = -1.0$ for the $({\equiv}FeO)_2VO_2^{-2}$ complex render the mono-protonated complex even more inner-spheric in comparison to the $\Delta z_0 = 0.4$ and $\Delta z_1 = -1.4$ values suggested by Larsson et al. (2017). The values of $\Delta z_0 = 0.65$ and $\Delta z_1 = -0.65$ for the $({\equiv}FeO)2VOOH^-$ complex, and $\Delta z_0 = 0.9$ and $\Delta z_1 = 0.1$ for the $({\equiv}FeO)_2V(OH)_2$ complex, respectively, were used same as suggested by Larsson et al. (2017). The thus fitted $\log K_{298}$ values at 25 °C of 14.8, 22.0, and 27.6, respectively, are similar to those found previously by Larsson et al. (2017). The respective fit parameters for other temperatures are compiled in Table 2. While the curves for the $({\equiv}FeO)_2V(OH)_2$ complex are negatively bend up to 50 °C, they become positively bend at 75 °C (Fig. S5d). The reason for this is not obvious but leads to an overprediction of the percentage of V adsorbed at slightly acidic conditions for the highest temperature studied. The quite good fit results ($R > 0.97$) for the vanadate $({\equiv}FeO)_2VO_2^{-2}$ and $({\equiv}FeO)_2VOOH^-$ complexes decrease linearly with temperature. The thus fitted $\log K_T$ values vs. T curves run nearly parallel to those of the inner-sphere molybdate adsorption reaction (Fig. 2). This indicates an exothermic adsorption reaction with increasing temperature, while an opposite behavior was found for the $({\equiv}FeO)_2V(OH)_2$ complex (reaction (7)), with a positive slope of the $\log K_T$ vs. T curve (Fig. 2). This indicates endothermic adsorption behavior as typical for cations (Machesky et al., 2023). Since this surface complex is formed by adsorption of the dioxovanadium(V) cation VO_2^+ (hidden in Eq. (7) by the formulation $HVO_4^{-2} + 3H^+ \leftrightarrow VO_2^+ + 2H_2O$), this behavior is not surprising. Adsorption of cations becomes stronger at higher temperatures and is therefore endothermic (i.e., $\Delta_r H$ values should be positive), in agreement with the observed decrease of pH_{pzc} of oxides with increasing temperature, as well as with enhanced cation-ligand complexation in bulk aqueous solutions at hydrothermal conditions (Kulik, 2006). While the contribution of the dioxovanadium (V) cation VO_2^+ can be neglected at room temperature, it becomes increasingly important with rising temperature at the expense of the $({\equiv}FeO)_2VOOH^-$ complex out-compensating the exothermic adsorption of the vanadate $({\equiv}FeO)_2VO_2^{-2}$ and $({\equiv}FeO)_2VOOH^-$ complexes (Fig. S5). In effect, the overall adsorption reaction becomes almost temperature-independent, despite the exclusively inner-sphere binding of the V species by the goethite adsorbent.

4. Conclusions

Despite the temperature corrections in $\log K$ of aqueous oxo-anion species formation (Table 1), no significant temperature effect was found in the end for adsorption by goethite of both molybdate and vanadate but due to different reasons. The adsorption of molybdate with a relatively steep adsorption envelope at circumneutral pH values is dominated by outer-sphere surface complexation. The CD-MUSIC model framework developed to quantify molybdate adsorption suggests that the $\log K_T$ values of the outer-sphere surface complexation do not change significantly with temperature in the range 10–75 °C studied. The model results suggest that the bi-dentate inner-sphere complex $({\equiv}FeO)_2MoO_2$ is dominant only at acidic pH conditions. Formation of this inner-sphere complex is, in fact, exothermic and more sensitive to temperature changes, and the formation reactions of the two inner-sphere vanadate oxo-anion complexes were found also to be exothermic. However, there is a formation reaction of a vanadyl oxo-cation surface complex, which is endothermic and counterbalances the exothermic oxo-anion reactions, resulting in a strong but almost temperature-independent V(V) adsorption reaction.

The model data can be used to predict both molybdate and vanadate adsorption behavior under various conditions, such as total concentrations, the amount of adsorbent, pH, ionic strength, and now also varying temperature. The $\log K_T$ values thus derived and compiled in Table 2 could readily be used by the Visual MINTEQ code at any temperature below 100 °C. The hypothesis conveyed that a temperature-induced increase in vanadate mobility observed during aquifer thermal energy storage (ATES) is due to a thermal desorption process appears to be less well-founded based on these results. An alternative hypothesis to be considered is microbial activity enhanced at increased temperatures, since the organic compounds in deep soil are highly vulnerable to decomposition under warming conditions potentially leading to the formation of DOM-bound V(IV) complexes at suboxic (Eh $\leq$ 0 mV) conditions. This may enhance vanadium mobility during ATES as well, but this alternative hypothesis should be verified by spectroscopic speciation analysis of the dissolved vanadium speciation for a full elucidation of the underlying scientific mechanisms governing vanadium mobility, an approach that has not been performed in any of the ATES studies reported so far.

Funding

The project was financed with resources of the German National Science Foundation (Grant No. DFG KE 508–31).

CRediT authorship contribution statement

Michael Kersten: Conceptualization, Data curation, Formal analysis, Funding acquisition, Investigation, Methodology, Project administration, Resources, Software, Supervision, Validation, Visualization, Writing – original draft, Writing – review & editing.

Declaration of competing interest

The authors declare that they have no known competing financial interests or personal relationships that could have appeared to influence the work reported in this paper.

Data availability

Data will be made available on request.

Acknowledgements

This study is dedicated to the late Prof. Dr. sc. Nataliya Vlasova from the Chuiko Institute of Surface Chemistry of the National Academy of Sciences of Ukraine in Kiev. Anna Dabizha assisted with pH titrations of goethite suspensions, while Regina Walter and Carolin Berg aided with the ICP-MS measurements. The draft has greatly benefited from insightful comments of the Associate Editor Jon Petter Gustafsson and an anonymous reviewer.

Appendix A. Supplementary data

Supplementary data to this article can be found online at https://doi.org/10.1016/j.apgeochem.2024.105907.

References

Abernathy, M.J., Schaefer, M.V., Ramirez, R., Garniwan, A., Lee, I., Zaera, F., Polizzotto, M.L., Ying, S.C., 2022. Vanadate retention by iron and manganese oxides. ACS Earth Space Chem. 6, 2041–2052.

Arena, G., Copat, C., Dimartine, A., Grasso, A., Fallico, R., Sciacca, S., Fiore, M., Ferrante, M., 2015. Determination of total vanadium and vanadium(V) in groundwater from Mt. Etna and estimate of daily intake of vanadium(V) through drinking water. J. Water Health 13, 522–530.

Bachmaf, S., Merkel, B.J., 2011. Estimating water chemistry parameters from experimental data using PEST with PHREEQC. Freiberg Online Geology 28, 18. tu-freiberg.de/sites/default/files/2023-08/fog_vol_28.pdf.

Bhattacharya, P., Claesson, M., Bundschuh, J., Sracek, O., Fagerberg, J., Jacks, G., Martin, R.A., Storniolo, A.d.R., Thir, J.M., 2006. Distribution and mobility of arsenic in the Río Dulce alluvial aquifers in Santiago del Estero Province, Argentina. Sci. Total Environ. 358, 97–120.

Boily, J.-F., 2012. Water structure and hydrogen bonding at goethite/water interfaces: implications for proton affinities. J. Phys. Chem. C 116, 4714–4724.

Bonte, M., van Breukelen, B.M., Stuyfzand, P.J., 2013. Temperature-induced impacts on groundwater quality and arsenic mobility in anoxic aquifer sediments used for both drinking water and shallow geothermal energy production. Water Res. 47, 5088–5100.

Bonte, M., Stuyfzand, P.J., van Breukelen, B.M., 2014. Reactive transport modeling of thermal column experiments to investigate the impacts of aquifer thermal energy storage on groundwater quality. Environ. Sci. Technol. 48, 12099–12107.

Borkovec, M., 1997. Origin of 1-pK and 2-pK models for ionizable water-solid interfaces. Langmuir 13, 2608–2613.

Brinza, L., Vu, H.P., Neamtu, M., Benning, L.G., 2019. Experimental and simulation results of the adsorption of Mo and V onto ferrihydrite. Sci. Rep. 9, 1365.

Bundschuh, J., Farias, B., Martin, R., Storniolo, A.d.R., Bhattacharya, P., Cortes, J., Bonorino, G., Albouy, R., 2004. Groundwater arsenic in the Chaco-Pampean Plain, Argentina: case study from Robles County, Santiago del Estero Province. Appl. Geochem. 19, 231–243.

Covington, A.K., Bates, R.G., Durst, R.A., 1985. Definition of pH scales, standard reference values, measurement of pH and related terminology. J. Pure Appl. Chem. 57, 531–542. https://www.degruyter.com/document/doi/10.1351/pac198557030531/html.

Coyte, R.M., Vengosh, A., 2020. Factors controlling the risks of co-occurrence of the redox-sensitive elements of arsenic, chromium, vanadium, and uranium in groundwater from the Eastern United States. Environ. Sci. Technol. 54, 4367–4375.

Craig, A.T., Amos, R.T., Gammon, P., 2021. Heated column experiments: a proxy for investigating the effects of *in situ* thermal recovery operations on groundwater geochemistry. J. Contam. Hydrol. 237, 103755.

Cruywagen, J.J., 2000. Protonation, oligomerization, and condensation reactions of vanadate(V), molybdate(VI), and tungstate(VI). Adv. Inorg. Chem. 49, 127–182.

Dabizha, A., Kersten, M., 2020. Exothermic adsorption of chromate by goethite. Appl. Geochem. 123, 104785.

Dabizha, A., Bahr, C., Kersten, M., 2020. Predicting breakthrough of vanadium in fixed-bed absorbent columns with complex groundwater chemistries: a multi-component granular ferric hydroxide-vanadate-arsenate-phosphate-silicic acid system. Water Res. X 9, 100061.

Davantès, A., Costa, D., Lefèvre, G., 2016. Molybdenum(VI) adsorption onto lepidocrocite (γ-FeOOH): in situ vibrational spectroscopy and DFT+U theoretical study. J. Phys. Chem. 120, 11871–11881.

Doherty, J., 2015. Calibration and Uncertainty Analysis for Complex Environmental Models. Watermark Numerical Computing, Brisbane, Australia. ISBN: 978-0-9943786-0-6. https://www.pesthomepage.org.

Gaboriaud, F., Ehrhardt, J.-J., 2003. Effects of different crystal faces on the surface charge of colloidal goethite (α-FeOOH) particles: an experimental and modeling study. Geochem. Cosmochim. Acta 67, 967–983.

Georgieva, I., Kersten, M., Tunega, D., 2020. Molecular modeling of MCPA herbicide adsorption by goethite (110) surface in dependence of pH. Theor. Chem. Acc. 139, 132.

Graedel, T.E., Miatto, A., 2023. Vanadium: a U.S. perspective on an understudied metal. Environ. Sci. Technol. 57, 8933–8942.

Gustafsson, J.P., 2003. Modelling molybdate and tungstate adsorption to ferrihydrite. Chem. Geol. 200, 105–115.

Gustafsson, J.P., Tiberg, C., 2015. Molybdenum binding to soil constituents in acid soils: an XAS and modeling study. Chem. Geol. 417, 279–288.

Gustafsson, J.P., 2019. Vanadium geochemistry in the biogeosphere – speciation, solid-solution interactions, and ecotoxicity. Appl. Geochem. 102, 1–25.

Gustafsson, J.P., 2022. Visual MINTEQ Ver. 4.0. https://vminteq.com/.

Härter, L., Kersten, M., Rißе, A., Poppe, R., Wieber, G., 2020. Vanadium in groundwater of the Eifel volcanic area, Germany. Grundwasser 25, 127–136 in German.

Halter, W.E., Pfeifer, H.-R., 2001. Arsenic(V) adsorption onto α-Al_2O_3 between 25 and 75 °C. Appl. Geochem. 16, 793–802.

Hamada, T., 1998. High vanadium content in Mt. Fuji groundwater and its relevance to the ancient biosphere. In: Nriagu, J.O. (Ed.), Vanadium in the Environment. Part 1: Chemistry and Biochemistry. Wiley & Sons, New York, pp. 97–123.

Han, J., Katz, L.E., 2019. Capturing the variable reactivity of goethites in surface complexation modeling by correlating model parameters with specific surface area. Geochem. Cosmochim. Acta 244, 248–263.

Harkness, J.S., Darrah, T.H., Moore, M.T., Whyte, C.J., Mathewson, P.D., Cook, T., Vengosh, A., 2017. Naturally occurring versus anthropogenic sources of elevated molybdenum in groundwater: evidence for geogenic contamination from southeast Wisconsin, United States. Environ. Sci. Technol. 51, 12190–12199.

Hiemstra, T., Van Riemsdijk, W.H., 1996. A surface structural approach to ion adsorption: the charge distribution (CD) model. J. Colloid Interface Sci. 179, 488–508.

Hiemstra, T., Van Riemsdijk, W.H., 2006. On the relationship between charge distribution, surface hydration, and the structure of the interface of metal hydroxides. J. Colloid Interface Sci. 301, 1–18.

Jelinek, L., Mištová, E., Kubeil, M., Stephan, H., 2021. Polyoxometalates in extraction and sorption processes. Solvent Extr. Ion Exch. 39, 455–476.

Kersten, M., Vlasova, N.N., 2009. Arsenite adsorption on goethite at elevated temperatures. Appl. Geochem. 24, 32–43.

Kersten, M., Vlasova, N.N., 2013. The influence of temperature on the selenate adsorption by goethite. J. Radiochim. Acta 101, 413–419.

Koh, D.-C., Chae, G.-T., Ryu, J.-S., Lee, S.-G., Ko, K.-S., 2016. Occurrence and mobility of major and trace elements in groundwater from pristine volcanic aquifers in Jeju Island, Korea. Appl. Geochem. 65, 87–102.

Kulik, D.A., 2000. Thermodynamic properties of surface species at the mineral-water interface under hypothetical conditions: a Gibbs energy minimization single-site 2pK_A triple-layer model of rutile in NaCl electrolyte to 250°C. Geochem. Cosmochim. Acta 64, 3161–3179.

Kulik, D.A., 2006. Standard molar Gibbs energies and activity coefficients of surface complexes on mineral-water interfaces (thermodynamic insights). In: Lützenkirchen, J. (Ed.), Surface Complexation Modelling, vol. 11. Elsevier Interface Science Technology Series, pp. 171–248.

Larsson, M.A., Persson, I., Sjöstedt, C., Gustafsson, J.P., 2017. Vanadate complexation to ferrihydrite: X-ray absorption spectroscopy and CD-MUSIC modelling. Environ. Chem. 14, 141–150.

Leiviskä, T., 2021. Vanadium (V) removal from water by sorption. In: Núñez-Delgado, A. (Ed.), Sorbent Materials for Controlling Environmental Pollution. Elsevier, pp. 543–571. https://doi.org/10.1016/B978-0-12-820042-1.00008-0.

Lüders, K., Hornbruch, G., Zarrabi, N., Heldt, S., Dahmke, A., Köber, R., 2021. Predictability of initial hydrogeochemical effects induced by short-term infiltration of ~75 °C hot water into a shallow glaciogenic aquifer. Water Res. X 13, 100121.

Lützenkirchen, J., Boily, J.F., Gunneriusson, L., Lövgren, L., Sjöberg, S., 2008. Protonation of different goethite surfaces – unified models for $NaNO_3$ and NaCl media. J. Colloid Interface Sci. 317, 155–165.

Lützenkirchen, J., Finck, N., 2019. Treatment of temperature dependence of interfacial speciation by speciation codes and temperature congruence of oxide surface charge. Appl. Geochem. 102, 26–33.

Machesky, M.L., Kubicki, J.D., Palmer, D.A., Wesolowski, D.J., 2023. Zn^{2+}, Co^{2+}, and Ni^{2+} adsorption at the rutile−water interface to 250 °C. ACS Earth Space Chem. 7, 1781–1790.

Mahringer, D., Zerelli, S.S., Dippon-Deißler, U., Ruhl, A.S., 2023. Biogenic amorphous ferric hydroxide as adsorbent for vanadium removal in drinking water production. Environ. Technol. Innovat. 32, 103239.

Naumann, R., Alexander-Weber, C., Eberhardt, R., Giera, J., Spitzer, P., 2002. Traceability of pH measurements by glass electrode cells: performance characteristic of pH electrodes by multi-point calibration. J. Anal. Bioanal. Chem. 374, 778–786.

Nicolli, H.B., Suriano, J.M., Gomezperal, M.A., Ferpozzi, L.H., Baleani, O.A., 1989. Groundwater contamination with arsenic and other trace elements in an area of the pampa, province of Córdoba, Argentina. Environ. Geol. Water Sci. 14, 3–16.

Oman, S.F., Camoes, M.F., Powell, K.J., Rajagopalan, R., Spitzer, P., 2007. Guidelines for potentiometric measurements in suspensions Part A. The suspension effect. Pure Appl. Chem. 79, 67–79.

Parnell, J., 2022. Vanadium for green energy: increasing demand but with health implications in volcanic terrains. GeoHealth 6, e2021GH000579. https://doi.org/10.1029/2021GH000579.

Peacock, C.L., Sherman, D.M., 2004. Vanadium(V) adsorption onto goethite (α-FeOOH) at pH 1.5 to 12: a surface complexation model based on ab initio molecular geometries and EXAFS spectroscopy. Geochem. Cosmochim. Acta 68, 1723–1733.

Samarin, A.S., Ivanov, A.V., Fedotov, S.S., 2023. Toward efficient recycling of vanadium phosphate-based sodium-ion batteries: a review. Cleanroom Technol. 5, 881–900.

Shaheen, S.M., Alessi, D.S., Tack, F.M.G., Ok, Y.S., Kim, K.-H., Gustafsson, J.P., Sparks, D. L., Rinklebe, J., 2019. Redox chemistry of vanadium in soils and sediments: interactions with colloidal materials, mobilization, speciation, and relevant environmental implications - a review. Adv. Colloid Interface Sci. 265, 1–13.

Smedley, P.L., Nicolli, H.B., 2014. Molybdenum distributions and controls in groundwater from the pampean aquifer of La pampa province, Argentina. In: Saji, V. S., Lopatin, S.I. (Eds.), Molybdenum and its Compounds: Applications, Electrochemical Properties and Geological Implications. Elsevier, pp. 399–416.

Smedley, P.L., Kinniburgh, D.G., 2017. Molybdenum in natural waters: a review of occurrence, distributions, and controls. Appl. Geochem. 84, 387–432.

Sverjensky, D.A., 2003. Standard states for the activities of mineral surface sites and species. Geochem. Cosmochim. Acta 67, 17–28.

Telfeyan, K., Johannesson, K.H., Mohajerin, T.J., Palmore, C.D., 2015. Vanadium geochemistry along groundwater flow paths in contrasting aquifers of the United States: carrizo Sand (Texas) and Oasis Valley (Nevada) aquifers. Chem. Geol. 410, 63–78.

Torres, J., Gonzatto, L., Peinado, G., Kremer, C., Kremer, E., 2014. Interaction of molybdenum(VI) oxyanions with +2 metal cations. J. Solut. Chem. 43, 1687–1700.

Vasseghian, Y., Rad, S.S., Vilas-Boas, J.A., Khataee, A., 2021. A global systematic review, meta-analysis, and risk assessment of the concentration of vanadium in drinking water resources. Chemosphere 267, 128904.
Vessey, C.J., Schmidt, M.P., Abdolahnezhad, M., Peak, D., Lindsay, M.B.J., 2020. Adsorption of (poly)vanadate onto ferrihydrite and hematite: an *in situ* ATR−FTIR study. ACS Earth Space Chem. 4, 641–649.
Villalobos, M., Cheney, M.A., Alcaraz-Cienfuegos, J., 2009. Goethite surface reactivity: II: a microscopic site-density model that describes its surface area-normalized variability. J. Colloid Interface Sci. 336, 412–422.
Wang, X., Sherman, D.M., 2021. Molecular speciation of Mo(VI) on goethite and its implications for molybdenum and its isotopic cycle in ocean. Geochem. Cosmochim. Acta 313, 116–132.
Weidner, E., Ciesielczyk, F., 2019. Removal of hazardous oxyanions from the environment using metal-oxide-based materials. Materials 12, 927.
White, D.J., Levy, L.S., 2021. Vanadium: environmental hazard or environmental opportunity? A perspective on some key research needs. Environ. Sci. Processes Impacts 23, 527–534.
Xu, N., Christodoulatos, C., Braida, W., 2006. Modeling the competitive effect of phosphate, sulfate, silicate, and tungstate anion on the adsorption of molybdate onto goethite. Chemosphere 64, 1325–1333.
Yang, P.-T., Wang, S.-L., 2021. Sorption and speciation of molybdate in soils: implications for molybdenum mobility and availability. J. Hazard Mater. 408, 124934.
Zhang, B., Zhang, H., He, J., Zhou, S., Dong, H., Rinklebe, J., Ok, Y.S., 2023. Vanadium in the environment: biogeochemistry and bioremediation. Environ. Sci. Technol. 57, 14770–14786.
Zhang, Y., Liu, X., Cheng, J., Lu, X., 2021. Surface acidity and As(V) complexation of iron oxyhydroxides: insights from first-principles molecular dynamics simulations. Environ. Sci. Technol. 55, 15921–15928.